World Journal of

Gastroenterology

Contents

ABOUT COVER

Editorial Board Member of *World Journal of Gastroenterology*, Hirayuki Enomoto, MD, PhD, Associate Professor, Division of Hepatobiliary and Pancreatic Disease, Department of Internal Medicine, Hyogo Medical University, Nishinomiya 663-8501, Hyogo, Japan. enomoto@hyo-med.ac.jp

AIMS AND SCOPE

The primary aim of *World Journal of Gastroenterology* (*WJG*, *World J Gastroenterol*) is to provide scholars and readers from various fields of gastroenterology and hepatology with a platform to publish high-quality basic and clinical research articles and communicate their research findings online. *WJG* mainly publishes articles reporting research results and findings obtained in the field of gastroenterology and hepatology and covering a wide range of topics including gastroenterology, hepatology, gastrointestinal endoscopy, gastrointestinal surgery, gastrointestinal oncology, and pediatric gastroenterology.

INDEXING/ABSTRACTING

The *WJG* is now abstracted and indexed in Science Citation Index Expanded (SCIE, also known as SciSearch®), Current Contents/Clinical Medicine, Journal Citation Reports, Index Medicus, MEDLINE, PubMed, PubMed Central, Scopus, Reference Citation Analysis, China National Knowledge Infrastructure, China Science and Technology Journal Database, and Superstar Journals Database. The 2022 edition of Journal Citation Reports® cites the 2021 impact factor (IF) for *WJG* as 5.374; IF without journal self cites: 5.187; 5-year IF: 5.715; Journal Citation Indicator: 0.84; Ranking: 31 among 93 journals in gastroenterology and hepatology; and Quartile category: Q2. The *WJG*'s CiteScore for 2021 is 8.1 and Scopus CiteScore rank 2021: Gastroenterology is 18/149.

RESPONSIBLE EDITORS FOR THIS ISSUE

Production Editor: *Yi-Xuan Cai*; **Production Department Director:** *Xiang Li*; **Editorial Office Director:** *Jia-Ru Fan*.

Ferroptosis inhibition attenuates inflammatory response in mice with acute hypertriglyceridemic pancreatitis

Yi-Teng Meng, Yi Zhou, Pei-Yu Han, Hong-Bo Ren

Yi-Teng Meng, Department of Gastroenterology, Shenzhen People's Hospital (The Second Clinical Medical College, Jinan University; The First Affiliated Hospital, Southern University of Science and Technology), Shenzhen 518020, Guangdong Province, China

Yi Zhou, Pei-Yu Han, Wuxi School of Medicine, Jiangnan University, Wuxi 214000, Jiangsu Province, China

Hong-Bo Ren, Department of Gastroenterology, Qilu Hospital, Jinan 250012, Shandong Province, China

Corresponding author: Hong-Bo Ren, PhD, Professor, Department of Gastroenterology, Qilu Hospital, No. 107 Wenhuaxi Road, Jinan 250012, Shandong Province, China. rhb2229@163.com

Abstract

BACKGROUND

Ferroptosis is involved in developing inflammatory diseases; yet, its role in acute hypertriglyceridemic pancreatitis (HTGP) remains unclear.

AIM

To explore whether ferroptosis is involved in the process of HTGP and elucidate its potential mechanisms.

METHODS

An HTGP mouse model was induced using intraperitoneal injection of P-407 and caerulein (CAE). Then, pancreatic tissues from the model animals were subjected to proteome sequencing analysis. The pathological changes and scores of the pancreas, lung, and kidney were determined using hematoxylin-eosin staining. The levels of serum amylase (AMY), triglyceride, and total cholesterol were measured with an automatic blood cell analyzer. Additionally, the serum levels of tumor necrosis factor (TNF)-α, interleukin (IL)-6, and IL-1β were determined by enzyme linked immunosorbent assay. Malonaldehyde (MDA), glutathione (GSH), and Fe^{2+} were detected in the pancreas. Finally, immunohistochemistry was performed to assess the expression of ferroptosis-related proteins.

RESULTS

Proteome sequencing revealed that ferroptosis was involved in the process of HTGP and that NADPH oxidase (NOX) 2 may participate in ferroptosis

regulation. Moreover, the levels of serum AMY, TNF-α, IL-6, and IL-1β were significantly increased, MDA and Fe^{2+} were upregulated, GSH and ferroptosis-related proteins were reduced, and the injury of the pancreas, lung, and kidney were aggravated in the P407 + CAE group compared to CAE and wild type groups (all $P < 0.05$). Notably, the inhibition of ferroptosis and NOX2 attenuated the pathological damage and the release of TNF-α, IL-6, and IL-1β in the serum of the mice.

CONCLUSION
Ferroptosis was found to have an important role in HTGP and may be considered a potential target for clinical treatment.

Core Tip: Ferroptosis is involved in the development of inflammatory diseases, but its relationship with acute hypertriglyceridemic pancreatitis (HTGP) remains unclear. This study discoverd ferroptosis is involved in the process of HTGP and therefore a potential target for clinical treatment.

INTRODUCTION

Hypertriglyceridemia is one of the leading causes of acute pancreatitis (AP). In China, the incidence rate of acute hypertriglyceridemic pancreatitis (HTGP) has increased from 13% in 2009 to 25.6% in 2013, and it is currently considered a second predominant type of AP[1-3]. Compared with AP caused by other causes, HTGP is associated with multiple organ dysfunction syndrome (MODS) and higher mortality[1, 4]. However, the underlying mechanisms of HTGP remain clear, and no effective treatments are available. Therefore, exploring the pathogenesis of HTGP and seeking more accurate therapeutic targets are of critical importance.

It is generally believed that excessive triglyceride (TG), which is hydrolyzed by pancreatic lipase, results in the release of damage-inducing free fatty acids (FFA), which then directly damage the pancreatic function and induce and amplify inflammatory responses through oxidative stress, aggravating multiple organ damage and leading to MODS[5-8]. In 2020, Rawla *et al*[9] found that when serum TG levels were higher than 1000 mg/dL, the incidence of AP was 5%, but when TG was over 2000 mg/dL, the incidence of AP increased to 10%-20%[9].

Previous studies have also revealed that various forms of regulated cell death (RCD), such as apoptosis and autophagy, are involved in the pathogenesis of AP[10-12]. Yet, the role of ferroptosis in HGAP is still not fully understood. Ferroptosis, as an iron-dependent form of non-apoptotic cell death first reported in 2012, is induced by excessive accumulation of peroxidized lipids and strictly regulated by glutathione peroxidase 4 (GPX4) and acyl-CoA synthetase long-chain family member 4[13-16]. Existing evidence suggests that the development of many diseases, including cancer, neurological diseases, ischemia-reperfusion injury, kidney injury, and cardiovascular diseases, is driven by ferroptosis[17-21]. In addition to altered iron homeostasis, the excessive production of reactive oxygen species (ROS) has also been reported as a key factor in ferroptosis induction[22].

Abnormal lipid metabolism is also considered to have an important role in the process of HTGP[4]. Meanwhile, FFA has been found to induce the excessive release of ROS and accumulation in the body [5]. Therefore, since abnormal lipid metabolism and ROS accumulation occur in both ferroptosis and HTGP, we hypothesized that ferroptosis might also participate in the process of HTGP. In the present study, we assessed the role of ferroptosis in HTGP through proteome sequencing. Then, we investigated the possible pathways and verified our results using animal experiments. This study provides new insides into the mechanism and treatment of HTGP.

MATERIALS AND METHODS

Materials and reagents

P-407 and caerulein (CAE) were purchased from Sigma Chemical (St. Louis, MO, United States). Ferrostatin-1 (Fer-1) and Vas2870 (Vas) were obtained from MedChemExpress (MCE, Monmouth Junction, NJ, United States). P-407 was solubilized in phosphate buffer solution (PBS) and stored at 4 °C. CAE, Fer-1, and Vas were solubilized in dimethyl sulfoxide and stored at 20 °C. Enzyme linked immunosorbent assay (ELISA) kits were obtained from Solarbio (Beijing, China).

Animals and modeling

Adult male C57BL/6 mice (25-30 g, 8-wk) were housed in a ventilated environment with a temperature of 22 ± 1 ℃, relative humidity of 50% ± 1%, and a light/dark cycle of 12/12 hr and given water and food ad libitum. After acclimatization, mice were randomly categorized into 4 groups (*n* = 4 per group): Control, P-407, AP (CAE), and HTGP (P-407 + CAE). The P-407 exposure group was intraperitoneally injected with a dosage of 0.6 g/kg body weight (bw) P-407[1,23]. Eight hours later, the AP group was intraperitoneally injected with a dosage of 100 μg/kg bw CAE 8 times (once every hour)[1,24]. The control group was injected with the same volume of PBS. After the last injection, all mice were alive. The animals were sacrificed and pancreas, lung, and kidney tissues were excised.

Serum assays

After the mice fasted for 16 h, Roche blood glucose meter was used to detect fasting blood glucose, and the collected blood from eyeballs was centrifuged at 4 °C, 3000 g for 10 min. The activities of the serum α-amylase (AMY), total cholesterol (TC), TG, aspartate transaminase (AST), and alanine aminotrans-ferase (ALT) in blood samples were measured by an automatic blood cell analyzer (Mindray, Shenzhen, China). Malonaldehyde (MDA), tumor necrosis factor (TNF)-α, interleukin (IL)-6, and IL-1β were detected by specific ELISA kits (Solarbio Science & Technology Co., Ltd, Beijing, China), following the manufacturer's instructions. The concentrations were expressed as pg/mL. The serum fasting insulin (FINS) levels were detected by a specific ELISA kit (Proteintech, Wuhan, China). The homeostasis model assessment insulin resistance index (HOMA-IR) = fasting blood glucose (FBG, mmol/L) × Fasting insulin (FINS, mIU/L)/22.5.

Glutathione detection

The Micro Reduced glutathione (GSH) Assay Kit was from Solarbio (Solarbio Science & Technology Co., Ltd, Beijing, China). Continuously dilute the standard product according to the corresponding concen-tration, and make the standard curve. Then, the supernatant of pancreas samples and total glutathione test solution were added into the 96-well plate successively, mixed, and incubated at 25 °C or room temperature for 5 min. 50 μL 0.5 mg/mL NADPH solution was added to per hole and mixed. The absorbance of each hole was measured immediately with an enzyme marker (λ = 412 nm). The total GSH content of each pore was obtained according to absorbance and standard curve. The sample is processed with GSH scavenger and GSH scavenger assistant in the kit to remove GSH, and the content of oxidized glutathione disulfide (GSSG) is measured, finally the content of reduced GSH is subtracted by total GSH and GSSG.

Fe^{2+} detection

Fe^{2+} in pancreas was detected according to the instructions in the Ferrous Ion Content Assay Kit (Solarbio Science & Technology Co., Ltd, Beijing, China). The absorbance was measured immediately with an enzyme marker (λ = 593 nm). The content of Fe^{2+} was obtained according to the concentration of standard substance and absorbance.

Malondialdehyde detection

MDA in pancreas was detected according to the instructions of MDA Content Assay Kit (Solarbio Science & Technology Co., Ltd, Beijing, China). After pretreatment, appropriate amount of supernatant was taken, and the absorbance of each group was measured at 532 nm. MDA content was obtained according to absorbance.

Histology and immunohistochemistry analyses

The tissue sections (pancreas, lung, and kidney) were cut into continuous slices. Hematoxylin–eosin (HE) staining was performed according to the Solarbio kit guidelines, and immunohistochemistry (IHC) analysis was conducted according to the Kangwei kit instructions. Images were acquired by Pannoramic MIDI (3DHISTECH). Brown-stained areas indicated immunoreactivity. Tissue sections were blindly evaluated by two pathologists based on previously reported criteria: The pathological injury of the pancreas was scored according to the edema, inflammation, hemorrhage, and necrosis of the pancreas [25]; the pathological score of the lung was measured on the basis of edema, neutrophil infiltration, and hemorrhage[26]; the pathological renal score was evaluated by the degree of tubulointerstitial injury

based on previously reported criteria[27].

Ferroptosis-related proteins (the light chain subunit solute carrier family 7 member 11 (SLC7A11) and GPX4 were determined by IHC analysis. Image J was used to quantify the expression of SLC7A11 and GPX4.

Protein extraction

The sample was ground with liquid nitrogen into cell powder and then transferred to a 5-mL centrifuge tube. After that, four volumes of lysis buffer (8 M urea, 1% protease inhibitor cocktail) were added to the cell powder, followed by sonication three times on ice using a high-intensity ultrasonic processor (Scientz). Next, the remaining debris was removed by centrifugation at 12000 g at 4 °C for 10 min. Finally, the supernatant was collected, and the protein concentration was determined with a Bicinchoninic Acid Assay kit according to the manufacturer's instructions.

Trypsin digestion

For digestion, the protein solution was reduced by 5 mmol/L dithiothreitol for 30 min at 56 °C and alkylated with 11 mmol/L iodoacetamide for 15 min at room temperature in darkness. The protein sample was then diluted by adding 100 mmol/L tetraethyl ammonium bromide to urea concentration < 2 M. Finally, trypsin was added at 1:50 trypsin-to-protein mass ratio for the first digestion overnight and 1:100 trypsin-to-protein mass ratio for a second 4 h digestion. Finally, the peptides were desalted using the C18 SPE column.

4D mass spectrometer

The tryptic peptides were dissolved in solvent A (0.1% formic acid, 2% acetonitrile/in water) and directly loaded onto a homemade reversed-phase analytical column (25 cm length, 75/100 µm inside diameter). Peptides were separated with a gradient from 6% to 24% solvent B (0.1% formic acid in acetonitrile) over 70 min, 24% to 35% in 14 min, and climbing to 80% in 3 min, then holding at 80% for the last 3 min, all at a constant flow rate of 450 nL/min on a nanoElute UHPLC system (Bruker Daltonics).

The peptides were subjected to a capillary source followed by the timsTOF Pro (Bruker Daltonics) mass spectrometry. The electrospray voltage applied was 1.60 kV. Precursors and fragments were analyzed at the TOF detector, with an MS/MS scan ranging from 100 to 1700 m/z. The timsTOF Pro was operated in parallel accumulation serial fragmentation (PASEF) mode. Precursors with charge states 0 to 5 were selected for fragmentation, and 10 PASEF-MS/MS scans were acquired per cycle. The dynamic exclusion was set to 30 s.

Database search

The resulting MS/MS data were processed using the MaxQuant search engine (v.1.6.15.0). Tandem mass spectra were searched against the mouse SwissProt database (17089 entries) concatenated with the reverse decoy database. Trypsin/P was specified as a cleavage enzyme allowing up to 2 missing cleavages. The mass tolerance for precursor ions was set as 20 ppm in the first search and 5 ppm in the main search, and the mass tolerance for fragment ions was set as 0.02 Da. Carbamidomethyl on Cys was specified as a fixed modification, and acetylation on protein N-terminal and oxidation on Met were specified as variable modifications. The false discovery rate was adjusted to < 1%. The data base is UniProt, the species-specific protein library is Mus_musculus_10090_SP_2021072. fasta. The proteomic analysis was performed by PTM Biolabs.

Principle component analysis

Principle component analysis (PCA) was conducted using R packages 'gmodels', 'ggplot2', and 'ggrepel'. The protein quantitative principal component (PC) analysis results of all samples were calculated. The degree of aggregation between samples in the figure represents the difference between samples.

Differentially expressed proteins analysis

The samples to be compared were selected, and the relative quantitative values of each protein in the repeated samples were taken as the difference multiple (fold change, FC). In order to judge the significance of the difference, the relative quantitative value of each protein in the samples of the comparison group was subjected to a *t*-test. The corresponding *P* value was calculated as the significance index. The default *P* value was < 0.05.

Gene Ontology enrichment analysis

Gene Ontology (GO) is used to express various properties of genes and gene products. GO annotations are divided into three categories: Biological Process, Cellular Component, and Molecular Function, which aim to explain the biological role of proteins from different perspectives. We performed differential protein enrichment analysis on a biological process in GO classification.

Kyoto Encyclopedia of Genes and Genomes pathway analysis

Kyoto Encyclopedia of Genes and Genomes (KEGG)[28] analysis was conducted using the 'cluster-Profiler' package[29] of R software. A previously described method was used[30].

Cluster analysis

According to Fisher's exact test obtained by the enrichment analysis, the related functions in different comparison groups were clustered using the hierarchical clustering method, and heatmaps were drawn. In the heatmaps, the horizontal direction of the heatmap represents different comparison groups, and the vertical direction indicates related functions enriched by differentially expressed proteins in different comparison groups. The color patches corresponding to the functional description of the enrichment of the differentially expressed proteins in different comparison groups indicate the degree of enrichment. Red color represents strong enrichment, and blue represents weak enrichment.

Statistical analysis

All data are expressed as mean ± SD. The statistical analyses were conducted using SPSS version 18.0 software, and the differences in data among the groups were analyzed using the unpaired Student *t*-test of variance test. $P < 0.05$ (2-tailed) was considered to indicate a statistically significant difference.

RESULTS

P-407 and CAE were successfully used to develop the mouse model of HTGP

The exposure of mice to P-407 and CAE for 48 h resulted in much higher TC and TG in the P-407 (model for hyperlipidemia) and P-407 + CAE (model for HTGP) groups than in the Ctrl and CAE (model for AP) groups (Figure 1A). A slight rise in the AMY level was seen in the CAE group, whereas in the P-407 + CAE group, a significant increase in the AMY level was detected compared to other groups (all $P < 0.05$, Figure 1B). In addition, an increase in AST and ALT levels were seen in the CAE-treated groups, but there was no difference between CAE and P-407 + CAE-treated groups ($P > 0.05$, Figure 1C). There was no change in HOMA-IR among different groups ($P > 0.05$, Figure 1D). Furthermore, in the CAE group, a minor injury was seen in the pancreas and kidney, whereas in the P-407 + CAE group, serious injuries were observed in the pancreas, lung, and kidney, which were detected by HE staining (Figure 1E-G). Also, in the P-407 + CAE group, high levels of serum TNF-α, IL-1β, and IL-6 were detected (Figure 1H). These results proved that P-407 and CAE mice models were successful.

Proteome profiling predicts the role of ferroptosis in P-407 + CAE-induced HTGP rather than AP

Next, proteome sequencing was used to compare the mechanisms of HTGP and AP. Samples of the same group were clustered together from both PCA and clustering analyses (Figure 2A and B). The CAE treatment caused the rightward movement of samples along the PC1, explaining 56.0% of the total variance. The P-407 + CAE treatment upward along PC2 explained 17.5% of the total variance (Figure 2A). Additionally, 190 proteins were downregulated, whereas 272 proteins were upregulated in the pairwise comparisons (CAE *vs* WT). Furthermore, 43 proteins were downregulated and 125 were upregulated when comparing P-407 + CAE and CAE groups (Figure 2C and D). These results suggested that AP and HTGP exert different effects on the pancreas.

　　GO analyses further showed that the acute inflammatory response was highly enchased in the P-407 + CAE group *vs* CAE group; this difference, however, was not evident when comparing CAE *vs* WT groups, which also confirmed that P-407 + CAE induces more severe pancreas injury than CAE (Figure 2E). Furthermore, KEGG pathway analyses also showed that upregulated proteins were weakly enriched for ferroptosis in the CAE group *vs* WT group but also strongly enriched for ferroptosis in the P-407 + CAE group *vs* CAE group (Figure 2F). These results suggest that ferroptosis occurs specifically in P-407 + CAE-induced HTGP.

### *Verification of P-407 + CAE-induced ferroptosis in mice*

To verify the results of proteome sequencing, we performed IHC staining of mouse pancreatic tissue. The SLC7A11 and GPX4 expression levels were significantly lower in the P-407 + CAE group than in the CAE group (all $P < 0.05$, Figure 3A and B). The MDA (Figure 3C) levels in the P-407 + CAE group were significantly higher than those in the CAE group ($P < 0.05$), while the GSH level in the P-407 + CAE group was significantly lower than that in CAE group ($P < 0.05$) (Figure 3D). The Fe^{2+} (Figure 3E) levels in the P-407 + CAE group were significantly higher than those in the CAE group ($P < 0.05$), too. This data indicates that P-407 + CAE induces ferroptosis in the pancreas of the mice.

HTGP can be attenuated through ferroptosis inhibition in mice

Since we had established that P-407 + CAE specifically induced ferroptosis in the pancreas of the mice, we further aimed to determine the role of ferroptosis in the regulation of HTGP. First, we used Fer-1 to inhibit ferroptosis[7,8]. The expression of GPX4 (Figure 4A) in the P-407 + CAE + Fer-1 group increased
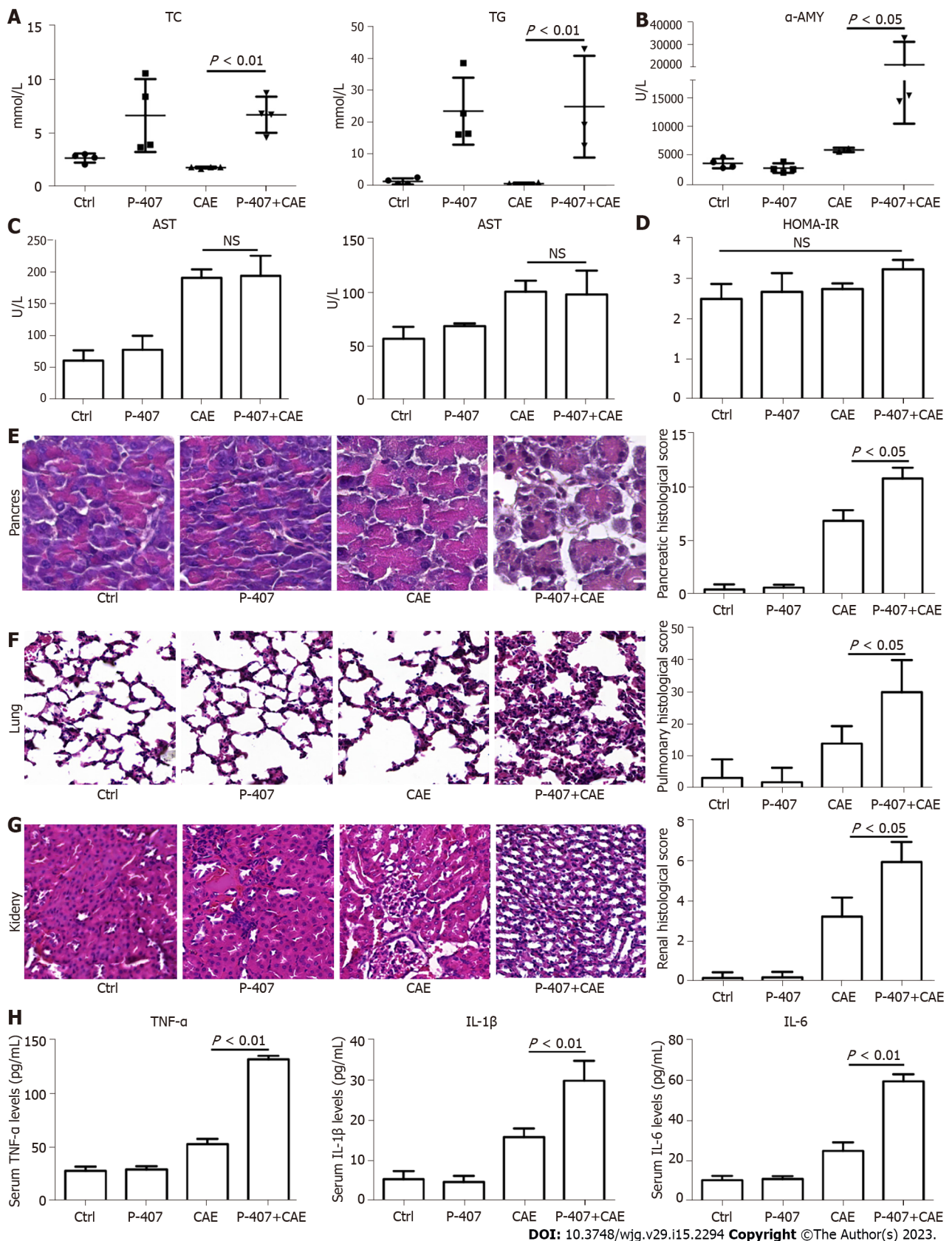
Figure 1 P-407 and caerulein-induced hypertriglyceridemic pancreatitis in mice (*n* = 4). A: Serum total cholesterol and triglyceride levels; B: Serum amylase; C: Alanine aminotransferase and Alanine aminotransferase levels; D: Homeostasis model assessment insulin resistance index levels in mice exposed to P-407 and caerulein (CAE); E: Hematoxylin–eosin (HE) staining and histological scores of the pancreas; F: HE staining and histological scores of the lung; G: HE staining and histological scores of the kidney; H: Serum Tumor necrosis factor-α, interleukin (IL)-1β, and IL-6 levels after P-407 and CAE exposure. AST: Aspartate transaminase; ALT: Alanine aminotransferase; HOMA-IR: Homeostasis model assessment insulin resistance index; HE: Hematoxylin–eosin; CAE: Caerulein; AMY: Amylase; TNF: Tumor necrosis factor; IL: Interleukin; NS: Not significant.

D

DOI: 10.3748/wjg.v29.i15.2294 Copyright ©The Author(s) 2023.
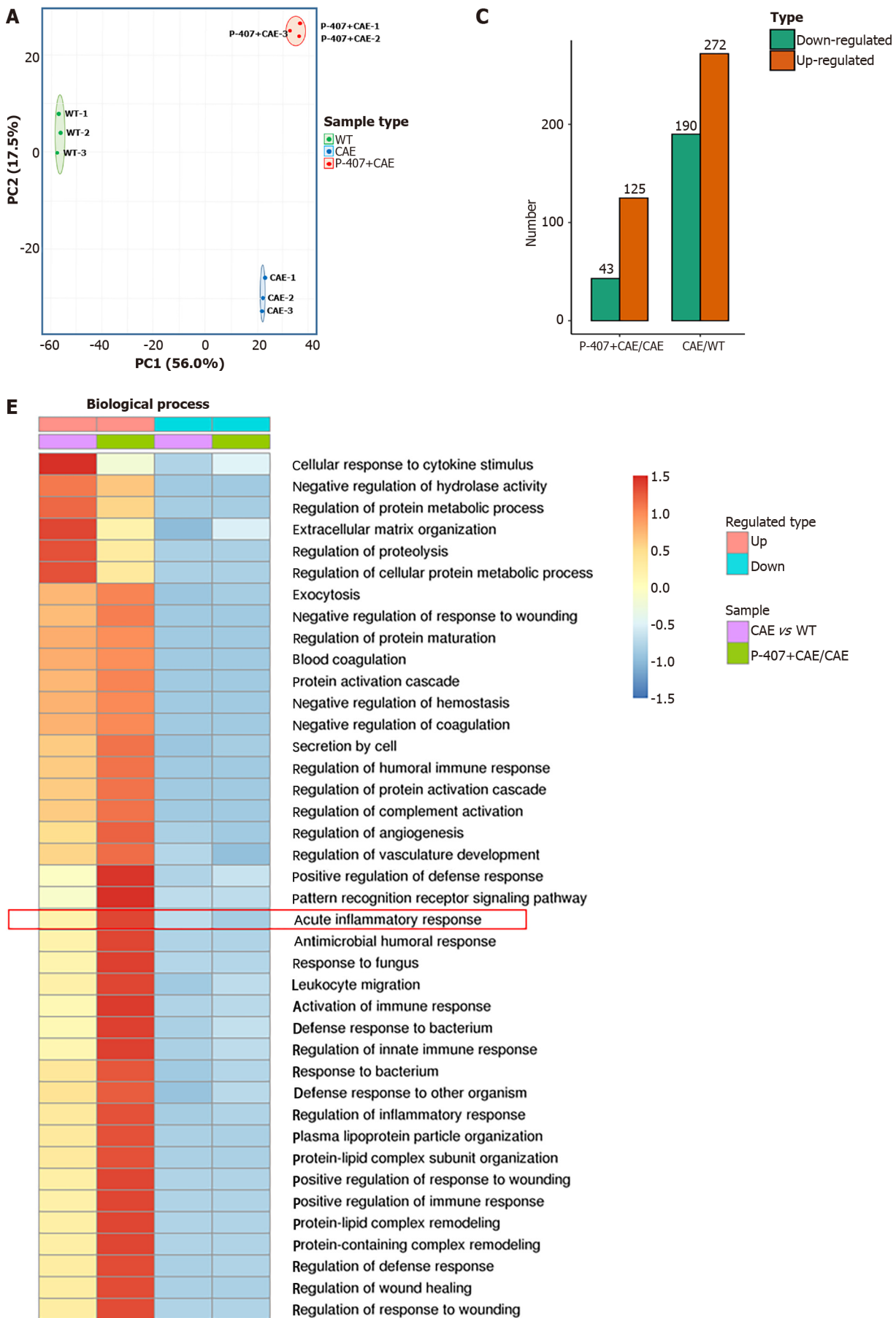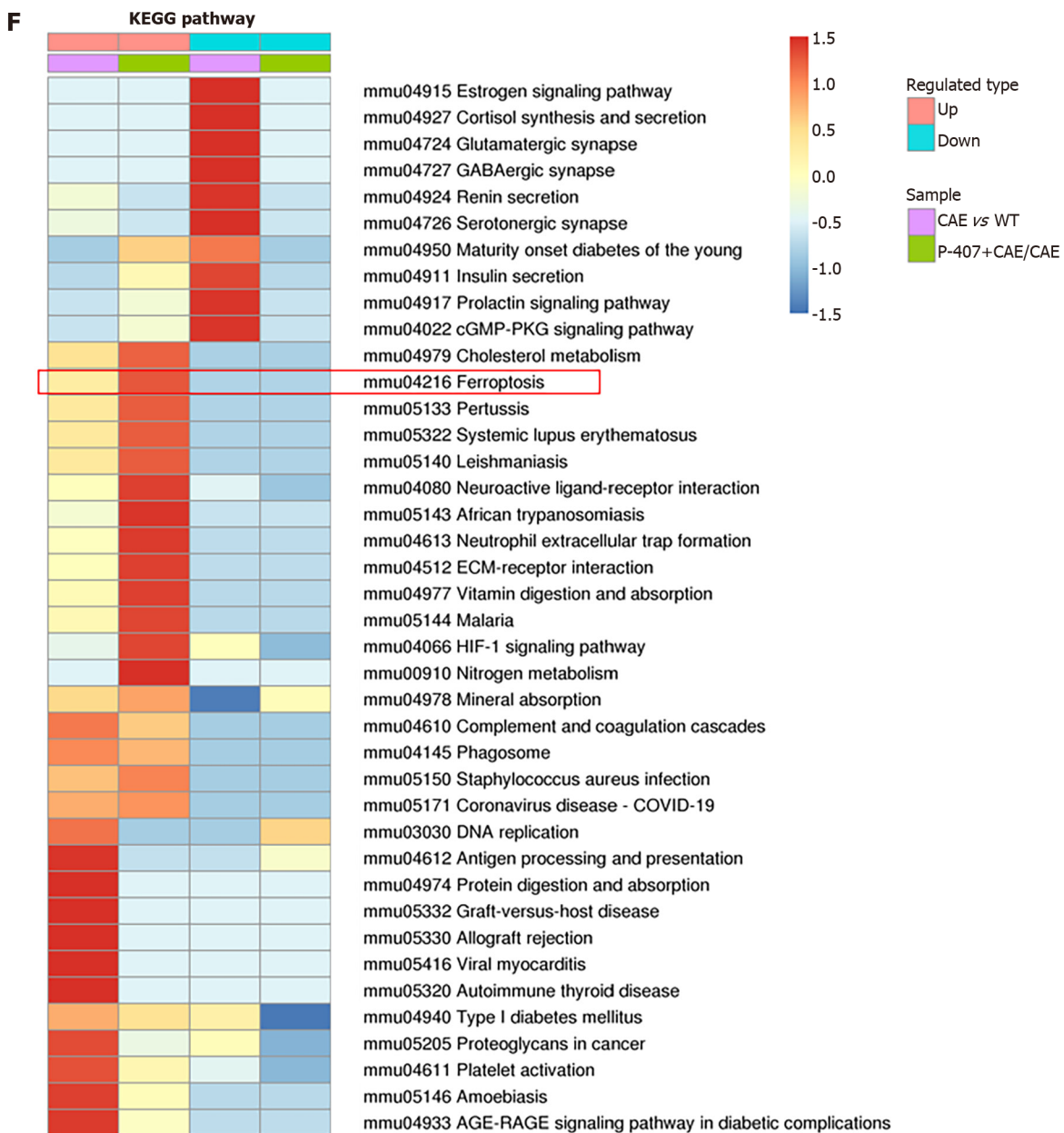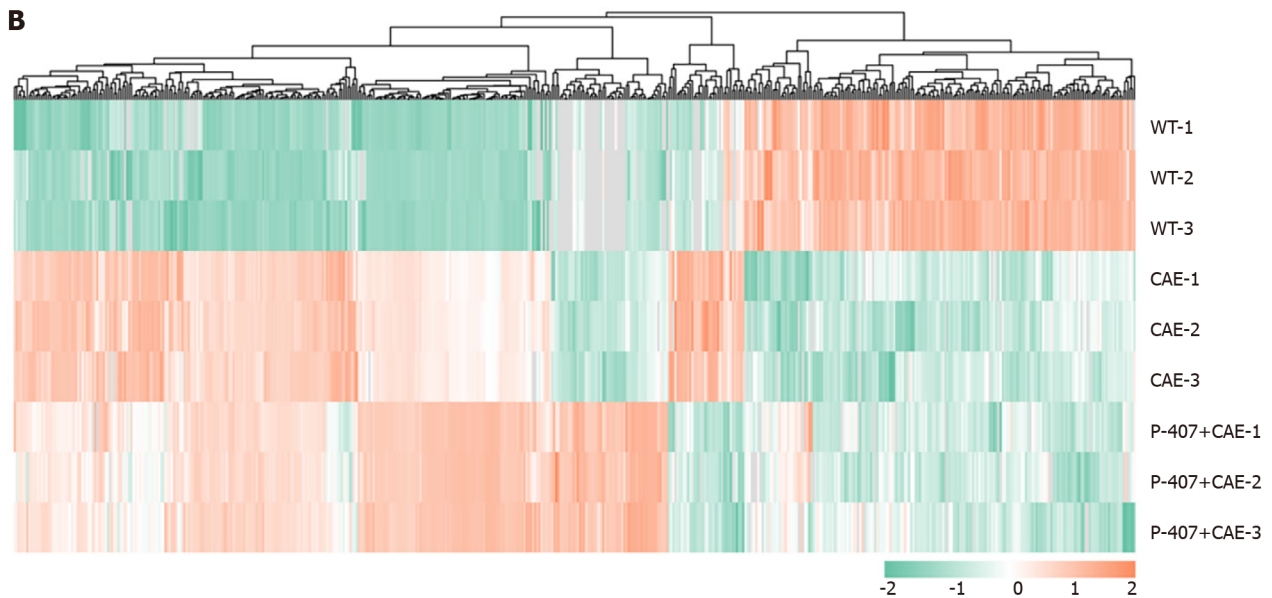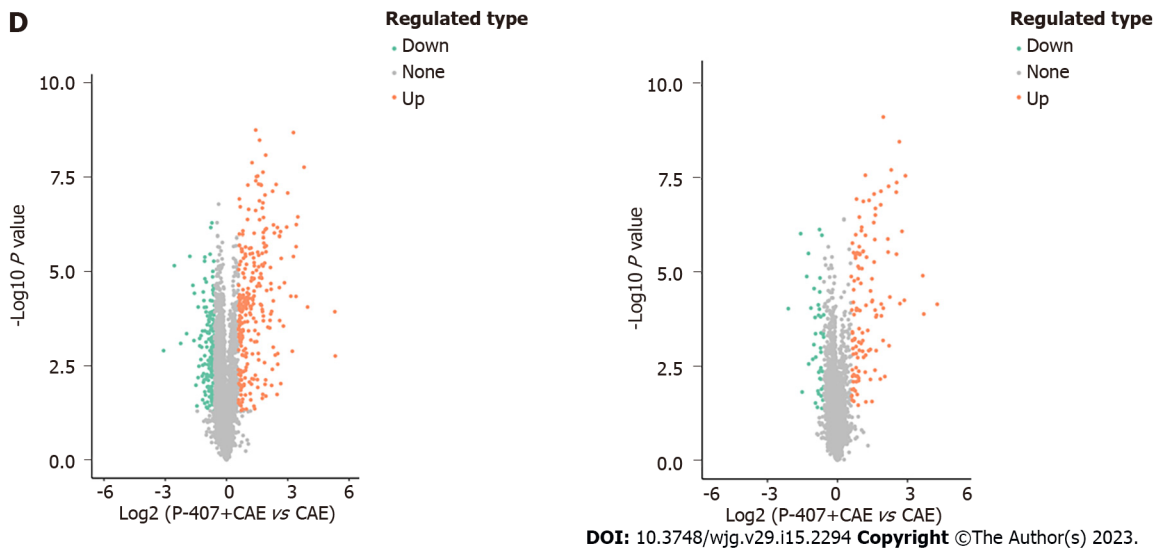
Figure 2 Effects of P-407 and caerulein on the pancreas revealed by proteome sequencing (*n* = 3). A: Principal component analysis; B: Heatmap showing relationships among different sample groups; C: Exhibition of changed protein numbers among the sample groups; D: Volcano plots showing proteins differentially expressed between sample groups; E: Biological process; F: Kyoto Encyclopedia of Genes and Genomes pathways enriched with proteins differentially expressed in pair-wise comparisons of 'CAE group' *vs* WT group'' and 'P-407 + CAE group' *vs* CAE group'. CAE: Caerulein; WT: Wide type; PC: Principal component.

DOI: 10.3748/wjg.v29.i15.2294 Copyright ©The Author(s) 2023.
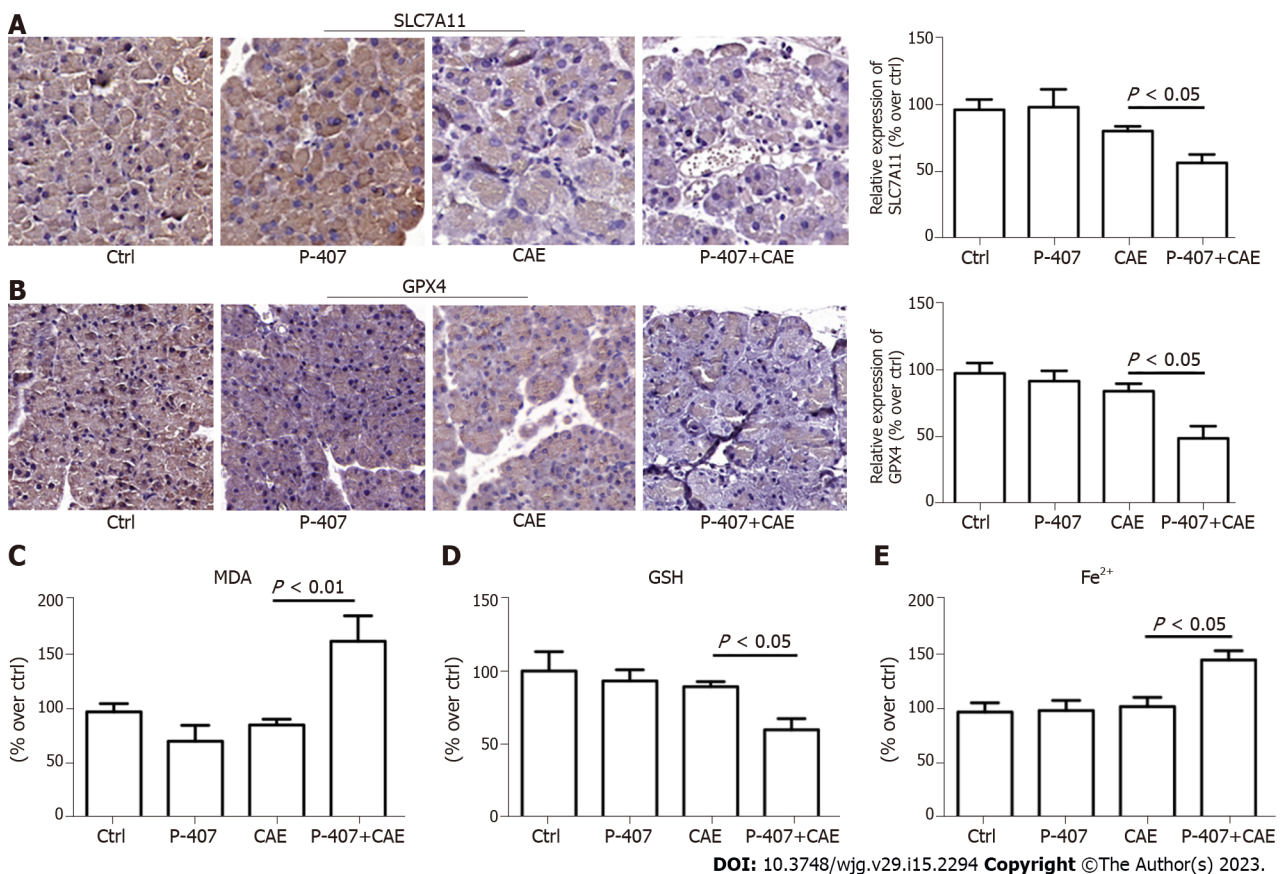
Figure 3 P-407 + Caerulein-induced pancreas ferroptosis in mice as established by immunohistochemistry (*n* = 4). A: Solute carrier family 7 member 11 in the pancreas tissues of the P-407 + Caerulein (CAE) group; B: Glutathione peroxidase 4 in the pancreas tissues of the P-407 + CAE group. The scale bar represents 50 mm; C: Malonaldehyde levels; D: Glutathione levels; E: Fe^{2+} levels in the pancreases of the mice in the P-407 + CAE group. CAE: Caerulein; SLC7A11: Solute carrier family 7 member 11; MDA: Malonaldehyde; GSH: Glutathione; GPX4: Glutathione peroxidase 4.

compared to P-407 + CAE group, while the MDA (Figure 4B) decreased to their normal range (all *P* < 0.05). The GSH level (Figure 4C) in the P-407 + CAE + Fer-1 group increased compared to P-407 + CAE group, while the Fe^{2+} (Figure 4D) decreased to their normal range (all *P* < 0.05). The histological scores of the pancreas, lung, and kidney in the P-407 + CAE + Fer-1 group were lower than those in the P-407 + CAE group (Figure 4E-G). The serum TNF-α, IL-1β, and IL-6 Levels in the P-407 + CAE + Fer-1 group were also lower than those in the P-407 + CAE group (all *P* < 0.05, Figure 4H). These results indicate that the inhibition of ferroptosis can attenuate the inflammatory response in mice with HTGP.

Inhibition of NADPH oxidase 2 can attenuate the inflammatory response in mice with HTGP through ferroptosis suppression

KEGG pathway analyses revealed overexpression of NADPH oxidase (NOX)2 in the enriched ferroptosis pathway in the P-407 + CAE group compared to the CAE group (Figure 5A and B). Next, we determined the role of NOX2 in regulating ferroptosis using Vas, an inhibitor of NOX2[7]. The expression of NOX2 was higher in the P-407 + CAE group than in the Ctrl group, while Vas significantly decreased the NOX2 expression level (*P* < 0.05, Figure 5C). In addition, MDA (Figure 5D) level decreased, GSH level increased (Figure 5E), Fe^{2+} (Figure 5F) level decreased and expression of GPX4 (Figure 5G) rebounded in the P-407 + CAE + Vas group compared to those in the P-407 + CAE group (*P* < 0.05). The histological scores of the pancreas, lung, and kidney in the P-407 + CAE + Vas group were lower than those in the P-407 + CAE group (all *P* < 0.05, Figure 5H-J). The serum TNF-α, IL-1β, and IL-6 Levels in the P-407 + CAE + Vas group were also lower than those in the P-407 + CAE group (all *P* < 0.05, Figure 5K). These results indicate that inhibition of NOX2 can attenuate the inflammatory response in mice with HTGP through attenuation of ferroptosis.

DISCUSSION

The early phase of HTGP is generally believed to be an unregulated inflammatory response or a cytokine storm that results in organ damage and death[31,32]. Pro-inflammatory cytokines, such as TNF-α, IL-6, and IL-1β, are considered pivotal mediators for initiating, amplifying, and perpetuating organ injury[33-35]. Therefore, timely blocking of the inflammatory response is considered critical for successful treatment.

As iron-dependent oxidative stress and lipid peroxidation are common features of ferroptosis and inflammatory diseases, ferroptosis, as a recognized form of RCD, has been reported to participate in the progression of inflammations[36]. Yet, its relationship with HTGP remains unclear. In the process of HTGP, abnormal lipid metabolism is also considered to have an important role, and FFA has been shown to induce the excessive release of ROS and accumulate in the body[4,5]. Previous studies have shown that the excessive production of ROS is a key factor for ferroptosis induction[22]. Therefore, we hypothesized that ferroptosis might also participate in the process of HTGP.

In this study, we found for the first time that ferroptosis has an important role in the process of HTGP, and its inhibition can attenuate the inflammatory response and improve prognosis in mice. To investigate these mechanisms, we induced a mouse model of HTGP by intraperitoneal injection of P-407 and CAE. Then, proteome sequencing predicted that ferroptosis is involved in the process of HTGP. To verify the results of proteome sequencing, we performed IHC staining of mouse pancreatic tissue. GSH, SLC7A11, and GPX4 expression levels were much lower in the P-407 + CAE group than in the AP group. Additionally, the MDA and Fe^{2+} level in the P-407 + CAE group was significantly higher than in the AP group. To further verify whether ferroptosis has a key role in regulating HTGP, we used Fer-1 to inhibit ferroptosis. The histological scores of pancreas and serum TNF-α, IL-1β, and IL-6 Levels in the P-407 + CAE + Fer-1 group were all significantly lower than those in the P-407 + CAE group.

Ma *et al*[21] found that the inhibition of ferroptosis attenuated acute kidney injury in rats with severe AP (SAP), suggesting that ferroptosis may participate in SAP, but there was no distinction between the types of SAP[21]. Furthermore, our KEGG pathway analyses revealed that the upregulated proteins were strongly enriched for ferroptosis in the P-407 + CAE group compared to the CAE group, implying that ferroptosis occurs specifically in the P-407 + CAE group. Based on this finding, we speculate that in the process of HTGP, abnormal lipid metabolism produces excessive ROS, which induces ferroptosis and aggravates damage to the pancreas and other organs.

NOX is a ROS-generating transmembrane flavoprotein enzyme that is widely distributed in pancreas and kidney tissues[37,38]. Studies have shown that excessive ROS produced by NOX can activate the NF-κB pathway, aggravate cell death, and regulate inflammation[39]. Yang *et al*[40] suggested that NOX could have an important role in HTGP-associated kidney injury through the Akt/GSK-3β pathway[40]. Moreover, Wang *et al*[41] found that NOX2 is activated in an AMPK-dependent manner to promote oxidative stress in a diabetic rat model, which in turn led to ferroptosis and aggravated myocardial ischemia-reperfusion injury[41]. Our KEGG pathway analyses also revealed overexpression of NOX2 in the enriched ferroptosis pathway in in the P-407 + CAE group compared to the CAE group. Next, we verified whether NOX2 has a key role in the regulation of ferroptosis using Vas, an inhibitor of NOX2. We found that the serum MDA level decreased, and the expression of GPX4 in the P-407 + CAE + Vas
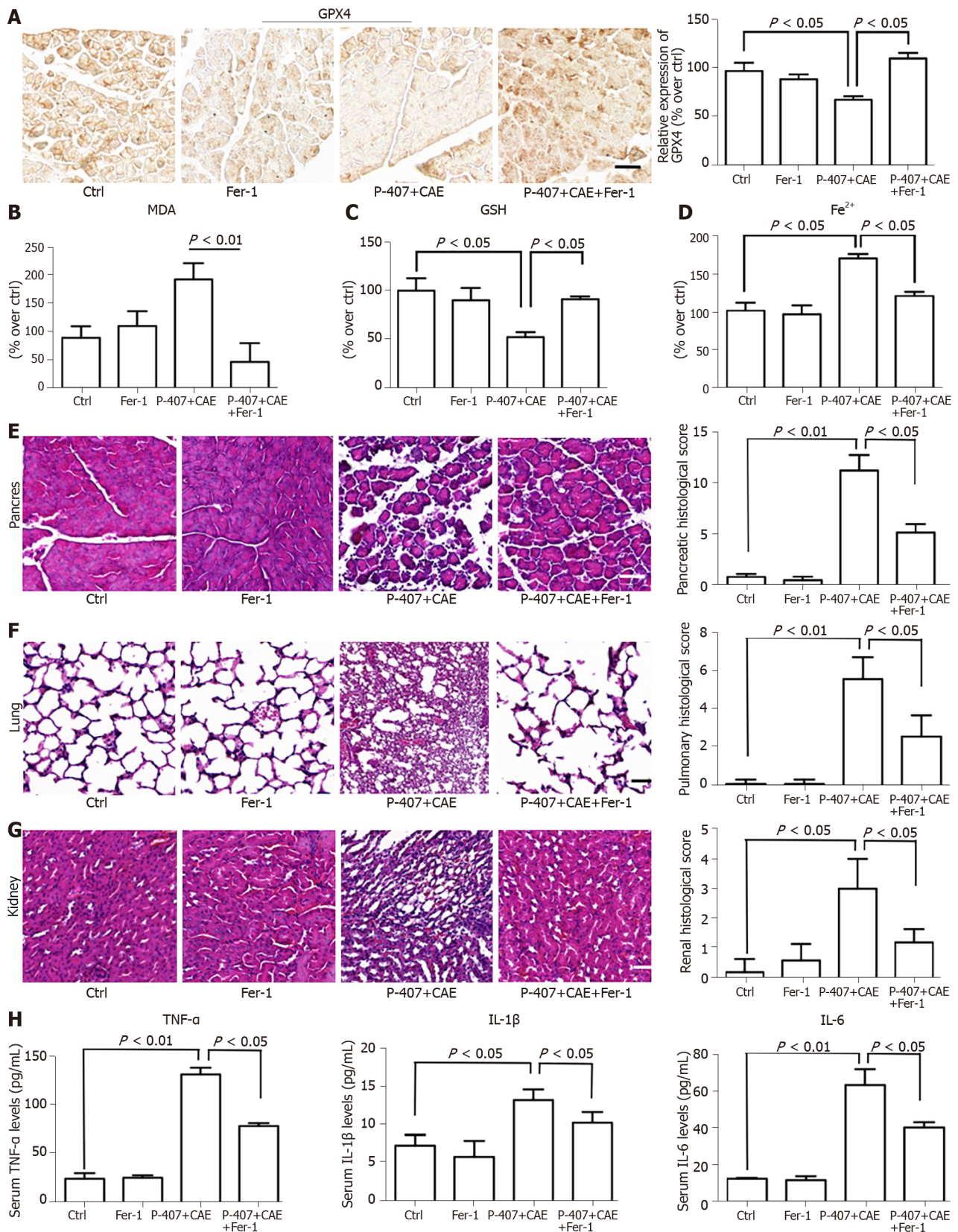
Figure 4 The inhibition of ferroptosis attenuated P-407 + Caerulein-induced hypertriglyceridemic pancreatitis in mice (*n* = 4). A: Immunohistochemistry for Glutathione peroxidase 4 in the pancreas tissues of the P-407 + Caerulein (CAE) and P-407 + CAE + Ferrostatin-1 (Fer-1) groups; B: The malonaldehyde levels; C: The glutathione levels; D: Fe^{2+} levels in pancreases of P-407 + CAE and P-407 + CAE + Fer-1 groups; E: Hematoxylin–eosin (HE) staining and histological scores of the pancreas; F: HE staining and histological scores of the lung; G: HE staining and histological scores of the kidney; H: Serum tumor necrosis factor-α, interleukin (IL)-1β, and IL-6 levels of the P-407 + CAE and P-407 + CAE + Fer-1 groups. NOX: NADPH oxidase; ROS: Reactive oxygen species; CAE: Caerulein; MDA: Malonaldehyde; Fer-1: Ferrostatin-1; GSH: Glutathione; GPX4: Glutathione peroxidase 4; TNF: Tumor necrosis factor; IL: Interleukin.
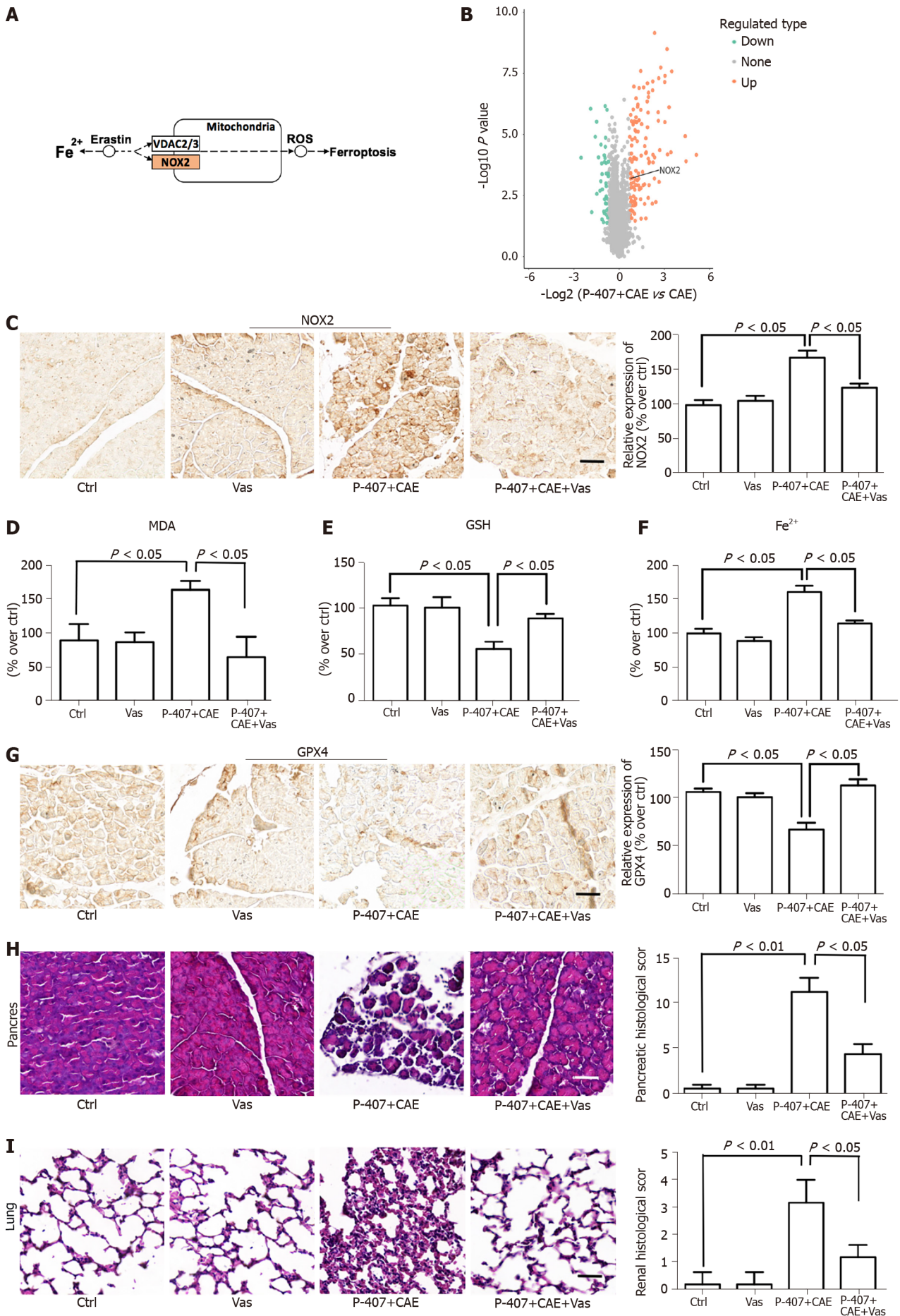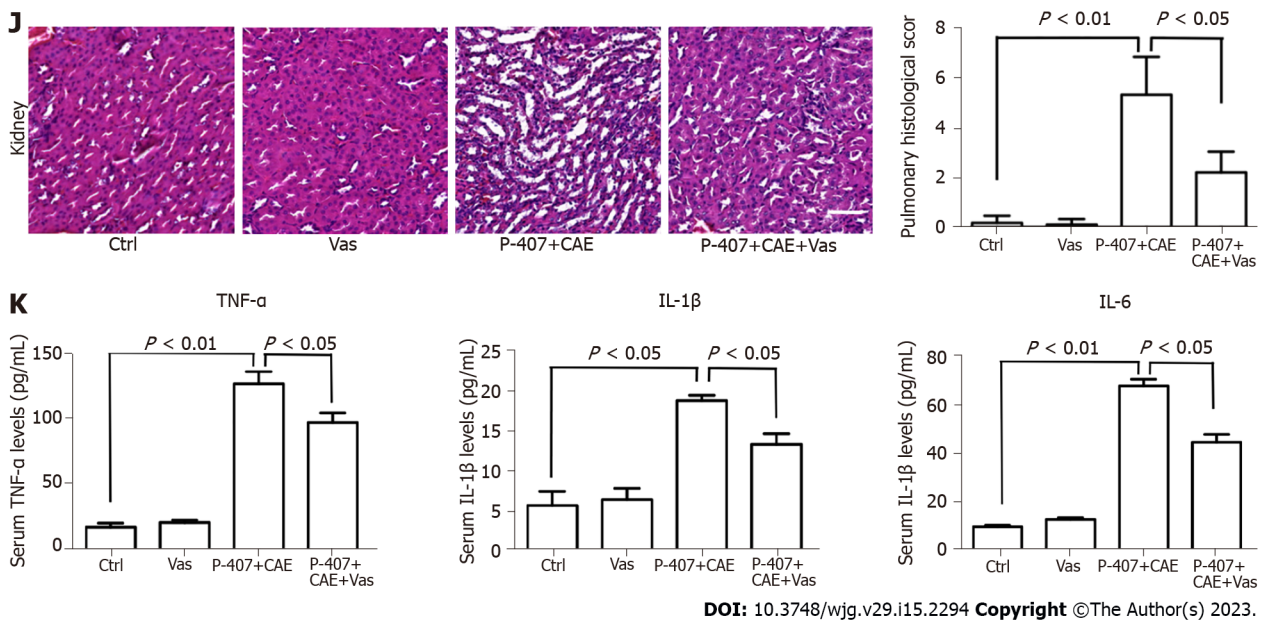
Figure 5 The inhibition of NADPH oxidase 2 attenuated hypertriglyceridemic pancreatitis through a ferroptosis reduction in mice (*n* = 4).
A: Kyoto Encyclopedia of Genes and Genomes pathways enriched with protein NADPH oxidase (NOX) 2 in comparison of P-407 + caerulein (CAE) group *vs* CAE group; B: Volcano plot showing the location of NOX2 in comparison of P-407 + CAE group *vs* CAE group; C: Immunohistochemistry (IHC) for NOX2 in the pancreas tissues of the P-407 + CAE and P-407 + CAE + Vas2870 (Vas) groups; D: The malonaldehyde levels; E: The glutathione levels; F: Fe^{2+} levels in the pancreases of the mice in the P-407 + CAE and P-407 + CAE + Vas groups; G: IHC for GPX4 in the pancreas tissues of the P-407 + CAE and P-407 + CAE + Vas groups; H: Hematoxylin–eosin (HE) staining and histological scores of the pancreas; I: HE staining and histological scores of the lung; J: HE staining and histological scores of the kidney; K: Serum TNF-α, IL-1β, and IL-6 levels of the P-407 + CAE and P-407 + CAE + Vas groups. The scale bar represents 50 mm. NOX: NADPH oxidase; ROS: Reactive oxygen species; CAE: Caerulein; Vas: Vas2870; MDA: Malonaldehyde; GSH: Glutathione; GPX4: Glutathione peroxidase 4; TNF: Tumor necrosis factor; IL: Interleukin.

group rebounded compared to the P-407 + CAE group. Meanwhile, the histological scores of the pancreas and the serum TNF-α, IL-1β, and IL-6 Levels in the P-407 + CAE + Vas group were significantly lower than those in the P-407 + CAE group. These results indicate that the inhibition of NOX2 attenuated HTGP through suppression of ferroptosis.

CONCLUSION

In summary, these data provide strong evidence that ferroptosis is involved in the process of HTGP and that NOX2 is a key point in the regulation of ferroptosis. The inhibition of ferroptosis and NOX2 attenuates the inflammatory response to improve patient outcomes. This discovery provides new insights into a better understanding of the pathogenesis of HTGP, which may be used as a novel therapeutic target in the future.

ARTICLE HIGHLIGHTS

Research background
Ferroptosis is involved in the development of inflammatory diseases, but its relationship with acute hypertriglyceridemic pancreatitis (HTGP) remains unclear.

Research motivation
HTGP has serious morbidity and high mortality. At present, there is no more effective method except symptomatic treatment. Therefore, exploring the pathogenesis of HTGP and seeking more accurate therapeutic targets are of critical importance.

Research objectives
This study aimed to explore whether ferroptosis is involved in the process of HTGP and elucidate its potential mechanisms in a mouse model.

Research methods

Pancreatic tissues from the model animals were subjected to proteome sequencing analysis. The pathological changes and scores of the pancreas, lung, and kidney were determined using hematoxylin–eosin staining. The levels of serum amylase, triglyceride, and total cholesterol were measured with an automatic blood cell analyzer. Additionally, the serum levels of tumor necrosis factor-α, interleukin (IL)-6, and IL-1β were determined by enzyme linked immunosorbent assay. Malonaldehyde, glutathione, and Fe^{2+} were detected in the pancreas. Finally, immunohistochemistry was performed to assess the expression of ferroptosis-related proteins.

Research results

Proteome sequencing revealed that ferroptosis was involved in the process of HTGP and that NADPH oxidase 2 may participate in ferroptosis regulation.

Research conclusions

Ferroptosis was found to have an important role in HTGP and may be considered a potential target for clinical treatment.

Research perspectives

This discovery provides new insights into a better understanding of the pathogenesis of HTGP, which may be used as a novel therapeutic target. However, the regulatory mechanism needs to be further explored in the future.

FOOTNOTES

Author contributions: Meng YT, Zhou Y, Han PY, and Ren HB designed the study; Meng YT, Zhou Y and Han PY participated in data collection and wrote the paper; Ren HB and Han PY were responsible for revising the manuscript, contributing the same to the paper; All the listed authors have contributed and approved the final manuscript.

Institutional animal care and use committee statement: This study was approved by the Ethics Committee of Scientific Research of Jinan University Application for Laboratory Animal Ethical Review, No. 20210303-06.

Conflict-of-interest statement: All the authors report no relevant conflicts of interest for this article.

Data sharing statement: No additional data are available.

Country/Territory of origin: China

ORCID number: Yi-Teng Meng 0000-0002-0413-9048; Pei-Yu Han 0000-0002-8753-2426; Hong-Bo Ren 0000-0002-7667-535X.

S-Editor: Li L
L-Editor: A
P-Editor: Yu HG

REFERENCES

1   **Yang AL**, McNabb-Baltar J. Hypertriglyceridemia and acute pancreatitis. *Pancreatology* 2020; **20**: 795-800 [PMID: 32571534 DOI: 10.1016/j.pan.2020.06.005]

2   **Jin M**, Bai X, Chen X, Zhang H, Lu B, Li Y, Lai Y, Qian J, Yang H. A 16-year trend of etiology in acute pancreatitis: The increasing proportion of hypertriglyceridemia-associated acute pancreatitis and its adverse effect on prognosis. *J Clin Lipidol* 2019; **13**: 947-953.e1 [PMID: 31735687 DOI: 10.1016/j.jacl.2019.09.005]

3   **Yin G**, Cang X, Yu G, Hu G, Ni J, Xiong J, Hu Y, Xing M, Chen C, Huang Y, Tang M, Zhao Y, Cheng G, Wan R, Wang S, Wang X. Different Clinical Presentations of Hyperlipidemic Acute Pancreatitis: A Retrospective Study. *Pancreas* 2015; **44**: 1105-1110 [PMID: 26348469 DOI: 10.1097/MPA.0000000000000403]

4   **Guo YY**, Li HX, Zhang Y, He WH. Hypertriglyceridemia-induced acute pancreatitis: progress on disease mechanisms and treatment modalities. *Discov Med* 2019; **27**: 101-109 [PMID: 30939294 DOI: 10.5114/pg.2014.45412]

5   **Wan J**, He W, Zhu Y, Zeng H, Liu P, Xia L, Lu N. Stratified analysis and clinical significance of elevated serum triglyceride levels in early acute pancreatitis: a retrospective study. *Lipids Health Dis* 2017; **16**: 124 [PMID: 28655321 DOI: 10.1186/s12944-017-0517-3]

6   **Schönfeld P**, Wieckowski MR, Lebiedzińska M, Wojtczak L. Mitochondrial fatty acid oxidation and oxidative stress: lack of reverse electron transfer-associated production of reactive oxygen species. *Biochim Biophys Acta* 2010; **1797**: 929-938 [PMID: 20085746 DOI: 10.1016/j.bbabio.2010.01.010]

7   **Criddle DN**, Murphy J, Fistetto G, Barrow S, Tepikin AV, Neoptolemos JP, Sutton R, Petersen OH. Fatty acid ethyl esters cause pancreatic calcium toxicity *via* inositol trisphosphate receptors and loss of ATP synthesis. *Gastroenterology* 2006; **130**: 781-793 [PMID: 16530519 DOI: 10.1053/j.gastro.2005.12.031]

8   **Maléth J**, Rakonczay Z Jr, Venglovecz V, Dolman NJ, Hegyi P. Central role of mitochondrial injury in the pathogenesis of acute pancreatitis. *Acta Physiol (Oxf)* 2013; **207**: 226-235 [PMID: 23167280 DOI: 10.1111/apha.12037]

9   **Rawla P**, Sunkara T, Thandra KC, Gaduputi V. Hypertriglyceridemia-induced pancreatitis: updated review of current treatment and preventive strategies. *Clin J Gastroenterol* 2018; **11**: 441-448 [PMID: 29923163 DOI: 10.1007/s12328-018-0881-1]

10   **Tan JH**, Cao RC, Zhou L, Zhou ZT, Chen HJ, Xu J, Chen XM, Jin YC, Lin JY, Qi ZC, Zeng JL, Li SJ, Luo M, Hu GD, Jin J, Zhang GW. EMC6 regulates acinar apoptosis *via* APAF1 in acute and chronic pancreatitis. *Cell Death Dis* 2020; **11**: 966 [PMID: 33177505 DOI: 10.1038/s41419-020-03177-3]

11   **Tang GX**, Yang MS, Xiang KM, Yang BC, Liu ZL, Zhao SP. MiR-20b-5p modulates inflammation, apoptosis and angiogenesis in severe acute pancreatitis through autophagy by targeting AKT3. *Autoimmunity* 2021; **54**: 460-470 [PMID: 34402705 DOI: 10.1080/08916934.2021.1953484]

12   **Gukovskaya AS**, Gukovsky I, Algül H, Habtezion A. Autophagy, Inflammation, and Immune Dysfunction in the Pathogenesis of Pancreatitis. *Gastroenterology* 2017; **153**: 1212-1226 [PMID: 28918190 DOI: 10.1053/j.gastro.2017.08.071]

13   **Dixon SJ**, Lemberg KM, Lamprecht MR, Skouta R, Zaitsev EM, Gleason CE, Patel DN, Bauer AJ, Cantley AM, Yang WS, Morrison B 3rd, Stockwell BR. Ferroptosis: an iron-dependent form of nonapoptotic cell death. *Cell* 2012; **149**: 1060-1072 [PMID: 22632970 DOI: 10.1016/j.cell.2012.03.042]

14   **Yang WS**, SriRamaratnam R, Welsch ME, Shimada K, Skouta R, Viswanathan VS, Cheah JH, Clemons PA, Shamji AF, Clish CB, Brown LM, Girotti AW, Cornish VW, Schreiber SL, Stockwell BR. Regulation of ferroptotic cancer cell death by GPX4. *Cell* 2014; **156**: 317-331 [PMID: 24439385 DOI: 10.1016/j.cell.2013.12.010]

15   **Doll S**, Proneth B, Tyurina YY, Panzilius E, Kobayashi S, Ingold I, Irmler M, Beckers J, Aichler M, Walch A, Prokisch H, Trümbach D, Mao G, Qu F, Bayir H, Füllekrug J, Scheel CH, Wurst W, Schick JA, Kagan VE, Angeli JP, Conrad M. ACSL4 dictates ferroptosis sensitivity by shaping cellular lipid composition. *Nat Chem Biol* 2017; **13**: 91-98 [PMID: 27842070 DOI: 10.1038/nchembio.2239]

16   **Black FO**. Response to Stockwell CW. Vestibular testing: Past, present, future. Br J Audiol 1997; 31: 387-398. *Br J Audiol* 1998; **32**: 255-257 [PMID: 9923988 DOI: 10.3109/03005364000000073]

17   **Lachaier E**, Louandre C, Godin C, Saidak Z, Baert M, Diouf M, Chauffert B, Galmiche A. Sorafenib induces ferroptosis in human cancer cell lines originating from different solid tumors. *Anticancer Res* 2014; **34**: 6417-6422 [PMID: 25368241]

18   **Masaldan S**, Bush AI, Devos D, Rolland AS, Moreau C. Striking while the iron is hot: Iron metabolism and ferroptosis in neurodegeneration. *Free Radic Biol Med* 2019; **133**: 221-233 [PMID: 30266679 DOI: 10.1016/j.freeradbiomed.2018.09.033]

19   **Tuo QZ**, Lei P, Jackman KA, Li XL, Xiong H, Liuyang ZY, Roisman L, Zhang ST, Ayton S, Wang Q, Crouch PJ, Ganio K, Wang XC, Pei L, Adlard PA, Lu YM, Cappai R, Wang JZ, Liu R, Bush AI. Tau-mediated iron export prevents ferroptotic damage after ischemic stroke. *Mol Psychiatry* 2017; **22**: 1520-1530 [PMID: 28886009 DOI: 10.1038/mp.2017.171]

20   **Fang X**, Ardehali H, Min J, Wang F. The molecular and metabolic landscape of iron and ferroptosis in cardiovascular disease. *Nat Rev Cardiol* 2023; **20**: 7-23 [PMID: 35788564 DOI: 10.1038/s41569-022-00735-4]

21   **Ma D**, Li C, Jiang P, Jiang Y, Wang J, Zhang D. Inhibition of Ferroptosis Attenuates Acute Kidney Injury in Rats with Severe Acute Pancreatitis. *Dig Dis Sci* 2021; **66**: 483-492 [PMID: 32219613 DOI: 10.1007/s10620-020-06225-2]

22   **Imai H**, Matsuoka M, Kumagai T, Sakamoto T, Koumura T. Lipid Peroxidation-Dependent Cell Death Regulated by GPx4 and Ferroptosis. *Curr Top Microbiol Immunol* 2017; **403**: 143-170 [PMID: 28204974 DOI: 10.1007/82_2016_508]

23   **Dai J**, Jiang M, Hu Y, Xiao J, Hu B, Xu J, Han X, Shen S, Li B, Wu Z, He Y, Ren Y, Wen L, Wang X, Hu G. Dysregulated SREBP1c/miR-153 signaling induced by hypertriglyceridemia worsens acute pancreatitis and delays tissue repair. *JCI Insight* 2021; **6** [PMID: 33491670 DOI: 10.1172/jci.insight.138584]

24   **Silva-Vaz P**, Abrantes AM, Castelo-Branco M, Gouveia A, Botelho MF, Tralhão JG. Murine Models of Acute Pancreatitis: A Critical Appraisal of Clinical Relevance. *Int J Mol Sci* 2019; **20** [PMID: 31181644 DOI: 10.3390/ijms20112794]

25   **Schmidt J**, Rattner DW, Lewandrowski K, Compton CC, Mandavilli U, Knoefel WT, Warshaw AL. A better model of acute pancreatitis for evaluating therapy. *Ann Surg* 1992; **215**: 44-56 [PMID: 1731649 DOI: 10.1097/00000658-199201000-00007]

26   **Matute-Bello G**, Winn RK, Jonas M, Chi EY, Martin TR, Liles WC. Fas (CD95) induces alveolar epithelial cell apoptosis in vivo: implications for acute pulmonary inflammation. *Am J Pathol* 2001; **158**: 153-161 [PMID: 11141488 DOI: 10.1016/s0002-9440(10)63953-3]

27   **Wu C**, Zou L, Shi S, Tong Z, Shen X, Yang D, Ke L, Li W, Li J. The role of hypertriglyceridemia for acute kidney injury in the course of acute pancreatitis and an animal model. *Pancreatology* 2017; **17**: 561-566 [PMID: 28647101 DOI: 10.1016/j.pan.2017.06.006]

28   **Kanehisa M**, Goto S. KEGG: kyoto encyclopedia of genes and genomes. *Nucleic Acids Res* 2000; **28**: 27-30 [PMID: 10592173 DOI: 10.1093/nar/28.1.27]

29   **Yu G**, Wang LG, Han Y, He QY. clusterProfiler: an R package for comparing biological themes among gene clusters. *OMICS* 2012; **16**: 284-287 [PMID: 22455463 DOI: 10.1089/omi.2011.0118]

30   **Han P**, Shen L, Nan N, Zhou R, Li T, Dai X. Cold Atmospheric Plasma Boosts Virus Multiplication *via* EGFR(Tyr1068) Phosphorylation-Mediated Control on Cell Mitophagy. *Int J Biol Sci* 2022; **18**: 3405-3420 [PMID: 35637956 DOI: 10.7150/ijbs.71983]

31   **Yao W**, Liao H, Pang M, Pan L, Guan Y, Huang X, Hei Z, Luo C, Ge M. Inhibition of the NADPH Oxidase Pathway Reduces Ferroptosis during Septic Renal Injury in Diabetic Mice. *Oxid Med Cell Longev* 2022; **2022**: 1193734 [PMID: 35265258 DOI: 10.1155/2022/1193734]

32   **Deng F**, Zhao BC, Yang X, Lin ZB, Sun QS, Wang YF, Yan ZZ, Liu WF, Li C, Hu JJ, Liu KX. The gut microbiota metabolite capsiate promotes Gpx4 expression by activating TRPV1 to inhibit intestinal ischemia reperfusion-induced ferroptosis. *Gut Microbes* 2021; **13**: 1-21 [PMID: 33779497 DOI: 10.1080/19490976.2021.1902719]

33   **Forsmark CE**, Vege SS, Wilcox CM. Acute Pancreatitis. *N Engl J Med* 2016; **375**: 1972-1981 [PMID: 27959604 DOI: 10.1056/nejmra1505202]

34   **Meng Y**, Sha S, Yang J, Ren H. Effects of Tec Tyrosine Kinase Inhibition on the Inflammatory Response of Severe Acute Pancreatitis-Associated Acute Lung Injury in Mice. *Dig Dis Sci* 2019; **64**: 2167-2176 [PMID: 30761473 DOI: 10.1007/s10620-019-05524-7]

35   **Yu QH**, Guo JF, Chen Y, Guo XR, Du YQ, Li ZS. Captopril pretreatment protects the lung against severe acute pancreatitis induced injury *via* inhibiting angiotensin II production and suppressing Rho/ROCK pathway. *Kaohsiung J Med Sci* 2016; **32**: 439-445 [PMID: 27638402 DOI: 10.1016/j.kjms.2016.07.008]

36   **Mao H**, Zhao Y, Li H, Lei L. Ferroptosis as an emerging target in inflammatory diseases. *Prog Biophys Mol Biol* 2020; **155**: 20-28 [PMID: 32311424 DOI: 10.1016/j.pbiomolbio.2020.04.001]

37   **Vermot A**, Petit-Härtlein I, Smith SME, Fieschi F. NADPH Oxidases (NOX): An Overview from Discovery, Molecular Mechanisms to Physiology and Pathology. *Antioxidants (Basel)* 2021; **10** [PMID: 34205998 DOI: 10.3390/antiox10060890]

38   **Elumalai S**, Karunakaran U, Moon JS, Won KC. NADPH Oxidase (NOX) Targeting in Diabetes: A Special Emphasis on Pancreatic β-Cell Dysfunction. *Cells* 2021; **10** [PMID: 34206537 DOI: 10.3390/cells10071573]

39   **Cao WL**, Xiang XH, Chen K, Xu W, Xia SH. Potential role of NADPH oxidase in pathogenesis of pancreatitis. *World J Gastrointest Pathophysiol* 2014; **5**: 169-177 [PMID: 25133019 DOI: 10.4291/wjgp.v5.i3.169]

40   **Yang X**, Zhao K, Deng W, Zhao L, Jin H, Mei F, Zhou Y, Li M, Wang W. Apocynin Attenuates Acute Kidney Injury and Inflammation in Rats with Acute Hypertriglyceridemic Pancreatitis. *Dig Dis Sci* 2020; **65**: 1735-1747 [PMID: 31617131 DOI: 10.1007/s10620-019-05892-0]

41   **Wang C**, Zhu L, Yuan W, Sun L, Xia Z, Zhang Z, Yao W. Diabetes aggravates myocardial ischaemia reperfusion injury *via* activating Nox2-related programmed cell death in an AMPK-dependent manner. *J Cell Mol Med* 2020; **24**: 6670-6679 [PMID: 32351005 DOI: 10.1111/jcmm.15318]